Supporting Information

Influence of surface coverage on the formation of 4,4'-bipyridinium (viologen) single molecular junctions

Henrry M. Osorio,[a,b,f] Santiago Martín,[a,c]* David C. Milan,[d] Alejandro González-Orive,[b] Josef B. G. Gluyas,[e] Simon J. Higgins,[d] Paul J. Low,[e]* Richard J. Nichols,[d]* and Pilar Cea[a,b]*

[a]   Departamento de Química Física, Facultad de Ciencias, Universidad de Zaragoza, 50009, Spain.

[b]   Instituto de Nanociencia de Aragón (INA), Fundación INA, and Laboratorio de Microscopias Avanzadas (LMA) C/ Mariano Esquilor s/n Campus Rio Ebro, 50018, Zaragoza, Spain.

[c]   Instituto de Ciencia de Materiales de Aragón (ICMA), Universidad de Zaragoza-CSIC, 50009 Zaragoza, Spain.

[d]   Department of Chemistry, University of Liverpool, Crown Street, Liverpool, L69 7ZD, United Kingdom.

[e]   School of Molecular Science, University of Western Australia, 35 Stirling Highway, Crawley, Perth, 6009, Australia.

[f]   Departamento de Física, Escuela Politécnica Nacional, Av. Ladrón de Guevara, E11-253, 170525 Quito, Ecuador.

Fabrication and Characterization of Langmuir and Langmuir-Blodgett (LB) films

Figure S1 shows a representative surface pressure versus area per molecule (π–A) isotherm of [1](BF$_4$)$_2$ on a pure-water subphase as well as a surface potential-area per molecule (ΔV-A) isotherm. The π–A isotherm obtained features a lift-off at approximately 1.4 nm^2·molecule^{-1} followed by a monotonous increase in the surface pressure upon compression process. A ΔV-A isotherm can often provide useful information relating to the molecular order within the monolayer, showing phase changes that are frequently more difficult to determine in the π-A isotherm. The ΔV-A isotherm presents an initial positive surface potential of ~150 mV consistent with the formation of a positively ionized monolayer at the air-water interface.[1] The fluctuations in the surface potential values observed at low surface pressures are related with the

presence of molecular domains which are randomly distributed at the air-water interface. At 0.60 nm$^2 \cdot$molecule^{-1}, which corresponds to a surface pressure of ca. 12 mN$\cdot$m^{-1}, an abrupt decrease of ΔV is observed which has been interpreted as due to the collapse of the monolayer in which the dipole moments of the molecules are randomly distributed in a three-dimensional arrangement.
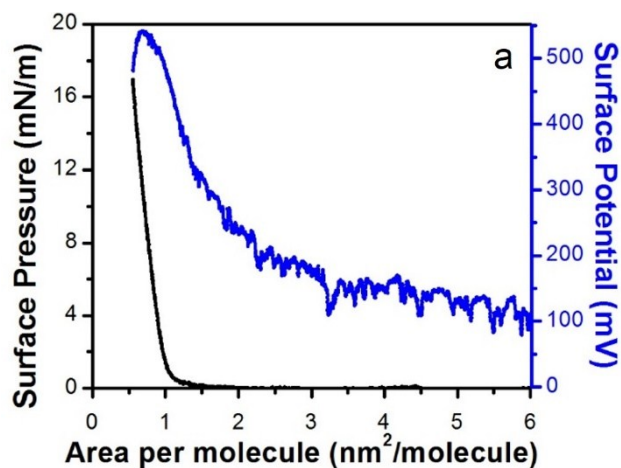
Figure S1. Surface pressure vs area per molecule ($\pi-A$) and surface potential vs area per molecule ($\Delta V-A$) isotherms for [**1**](BF$_4$)$_2$ recorded at 20 °C.

Brewster Angle Microscopy (BAM) images shown in Figure S2 indicate that a homogeneous film free of three dimensional aggregates is formed. Additionally, the increase in the brightness of the images upon compression indicates a more vertical disposition of the molecules in the monolayer as the surface pressure increases. At surface pressures beyond 12 mN$\cdot$m^{-1} some stripes in the monolayer can already be observed confirming local collapse in the film.
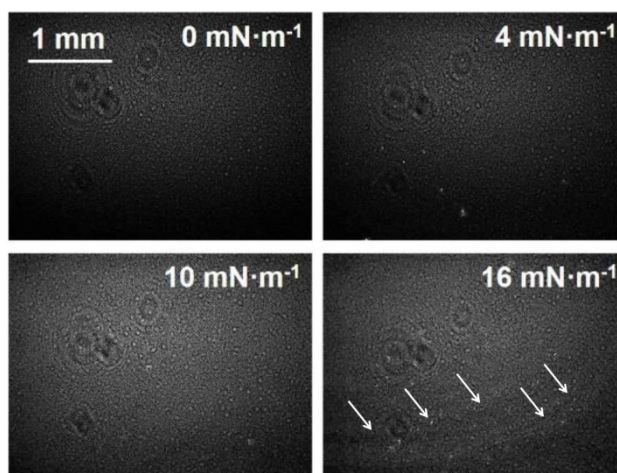
Figure S2. BAM images of [**1**](BF$_4$)$_2$ recorded during the compression process at the indicated surface pressures.

The molecular orientation of **1**$^{2+}$ at the air-water interface was investigated *in situ* by UV-Vis reflection spectroscopy using the reflection of unpolarized light under normal incidence. Normalized reflection spectra ($\Delta R_{norm}=\Delta R \cdot Area\ per\ molecule$, in which ΔR is the reflection) recorded at different values of the area per molecule upon the compression process are presented in Figure S3. The absorption spectrum of **1**$^{2+}$ (7.5·10^{-6} M in CHCl$_3$:EtOH, 3:1) is also presented for comparison purposes. The spectrum of the solution shows the presence of two peaks at 257 and 268 nm which are attributable to the π-π* electronic transition of the chromophore.[2] The reflection spectra show one well defined peak at 268 nm, accompanied by a shoulder at 257 nm. Importantly, in the reflection spectra the intensity of the peak at 268 nm decreases as the area per molecule decreases. The decrease in the intensity at 268 nm upon compression is consistent with an increase in the tilt angle of the viologen moiety with respect to the water surface, i.e. a progressive orientation of the viologen group occurs as also was concluded from the BAM images. This result is in good agreement with previous observations for other viologen derivatives assembled in LB films.[3]
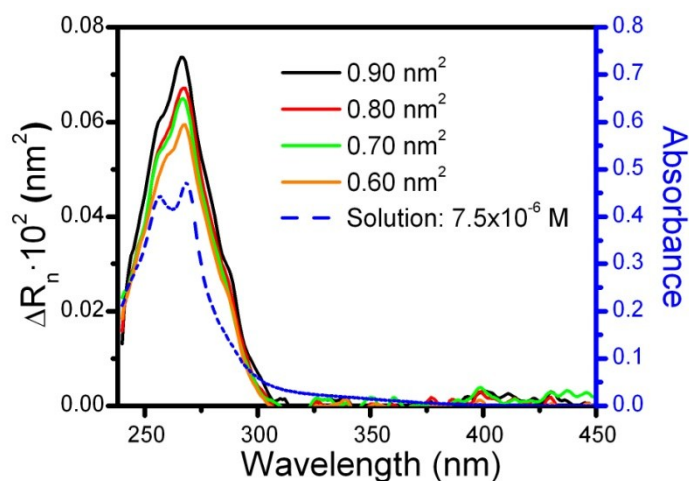
Figure S3. Normalized reflection spectra at different area per molecule values upon compression process of [**1**](BF$_4$)$_2$ and absorption spectrum of a 7.5×10^{-6} M solution of [**1**](BF$_4$)$_2$ in CHCl$_3$:EtOH 3:1.

Langmuir monolayers were transferred onto solid substrates to form Langmuir-Blodgett (LB) films by the vertical dipping method with the hydrophilic substrates initially immersed in the water subphase. Atomic force microscopy (AFM) was used to study

the morphology of the obtained films as well as to determine its homogeneity and quality in an attempt to find the optimum surface pressure of transference. Thus, monolayers of [1](BF$_4$)$_2$ were deposited onto freshly cleaved mica substrates at different surface pressures of transference. Figure S4 shows some representative AFM images together with their respective section analysis profiles. AFM results indicate that monolayers of [1](BF$_4$)$_2$ deposited at 10 mN·m^{-1} are more homogeneous and present a lower root mean square (RMS) roughness value with respect to those transferred at 6 and 14 mN·m^{-1}. In addition, the image corresponding to films transferred at 14 mN·m^{-1} is characterized by the presence of some irregular domains exhibiting a variety of height values. This result is in good agreement with the ΔV-A isotherm, which indicates the occurrence of local collapses at surfaces pressures beyond 12 mN·m^{-1}.
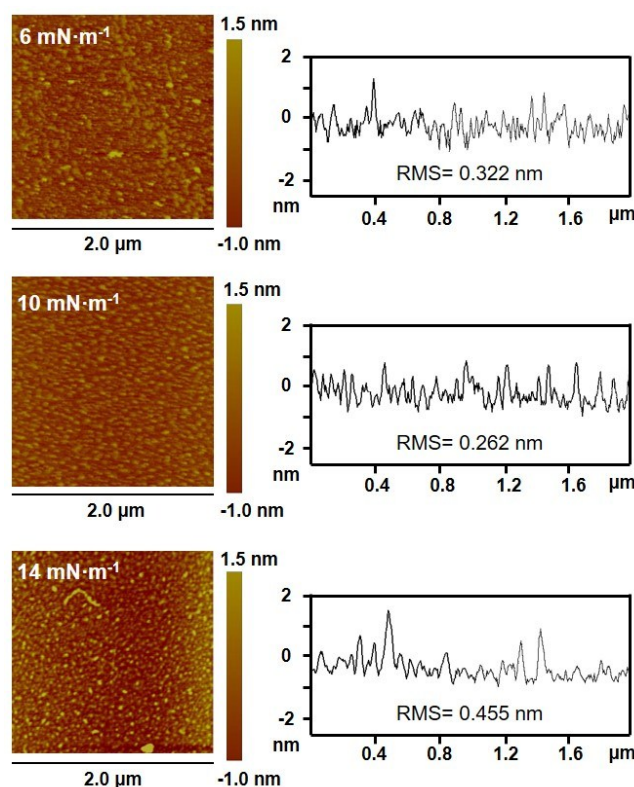
Figure S4. AFM images (left) and section analysis profile (right) of a one-layer LB film of [1](BF$_4$)$_2$ deposited onto freshly cleaved mica substrates at the indicated surface pressures of transference.

The transfer ratio at 10 mN·m^{-1} is close to unity as determined by the decrease in the area per molecule upon the transference process during the transference process. This deposition rate was also assessed using a quartz crystal microbalance (QCM). Thus, the

frequency change (Δf) for a QCM quartz resonator before and after the deposition process was determined. Taking into account the Sauerbrey equation:[4]

$$\Delta f = -\frac{2 \cdot f_0^2 \cdot \Delta m}{A \cdot \rho_q^{1/2} \cdot \mu_q^{1/2}} \qquad (1)$$

where f_0 is the fundamental resonant frequency of 5 MHz, Δm (g) is the mass change, A is the electrode area, ρ_q is the density of the quartz (2.65 g·cm⁻³), μ_q is the shear modulus (2.95·10¹¹ dyn·cm⁻²), the obtained surface coverage (Γ) is 2.0·10⁻¹⁰ mol·cm⁻², which is in good agreement with the surface density, 2.3·10⁻¹⁰ mol·cm⁻², determined from the molecular area of [1](BF₄)₂ at the air-water interface at 10 mN·m⁻¹.

The UV-vis absorption spectrum of the LB film of [1](BF₄)₂ transferred onto quartz substrates at 10 mN·m⁻¹ during the upstroke of the substrate was recorded (Figure S5) in order to obtain additional information about the molecular arrangement of [1](BF₄)₂ in LB films. The apparent molar absorptivities (ε_{app}) were calculated as described elsewhere[5] using Equations (2) and (3) for the monolayer at the air-water interface and the transferred LB films, respectively.

$$\varepsilon_{app} = \frac{\Delta R}{2.303 \cdot 10^3 \cdot \Gamma \cdot \sqrt{R_w}}$$

$$(2)$$

$$\varepsilon_{app} = \frac{A_b}{1000 \cdot \Gamma}$$

$$(3)$$

where Γ is the surface density in mol·cm⁻², R_w is the reflectivity of water (R_w=0.02) and A_b is the absorbance. The UV-vis absorption spectrum of the LB film exhibits an analogous profile to the reflection spectrum of the Langmuir film at 10 mN·m⁻¹. This result reveals that the molecular organization is maintained upon the transference process.
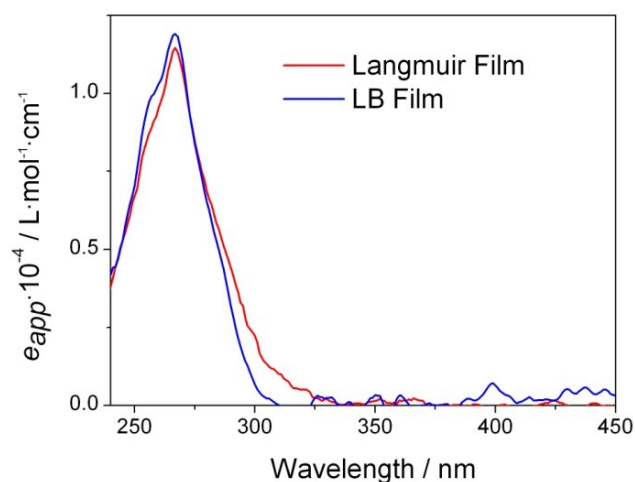
Figure S4. Apparent molar absorptivity vs. wavelength for a Langmuir film of [**1**](BF$_4$)$_2$ at 10 mN·m^{-1} and a LB monolayer transferred at 10 mN·m^{-1} onto a quartz substrate.

The electrochemical behavior of the densely packed LB films of [**1**](BF$_4$)$_2$ transferred at 10 mN·m^{-1} was studied and presented in Figure S5. The gold substrate covered by the LB films of [**1**](BF$_4$)$_2$ was used as the working electrode in an electrochemical cell in which the counter electrode was a Pt electrode and the reference electrode was an Ag/AgCl, KCl (3M), electrode. The electrochemical cell was filled with a 0.005 M KClO$_4$ aqueous solution and a nitrogen flux was used to purge any oxygen in the system. The first and second reduction peaks of the viologen – corresponding to the formation of the cation radical (P1) and the neutral species (P2) respectively – can be clearly observed in Figure S5. The corresponding oxidation peaks, labelled as P'1 and P'2, can also be seen. For comparison purposes the electrochemical behavior of a low coverage self-assembled monolayer was also studied. A very similar electrochemical behavior was observed.
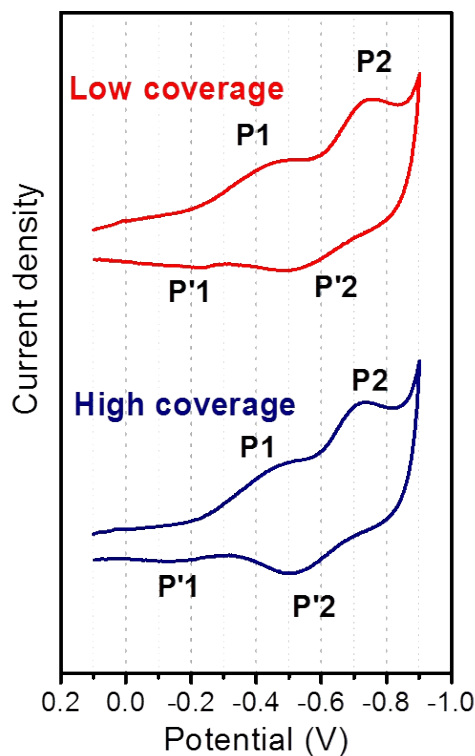
Figure S5. Cyclic voltammograms of an LB film, high coverage, of [**1**](BF$_4$)$_2$ and a low coverage film of the same compound. The scan rate was 0.2 V·s^{-1} at 20 °C and the initial scan direction was negative.

Figure S6 shows the X-ray photoelectron spectrum (XPS) of a Langmuir film of [**1**](BF$_4$)$_2$ transferred at 10 mN·m^{-1} as well as the XPS of [**1**](BF$_4$)$_2$ powder. The XPS of the LB film in the N 1s region shows three peaks at 401.3, 399.9 and 399.1 eV whose relative intensities depend on the XPS irradiation time. The peak at 401.3 has been attributed previously to the nitrogen in the viologen dication species[6] while the peaks at lower energy densities have been unambiguously assigned in the literature to the N in the viologen cation radical and neutral viologen that result from the so-called dry reduction of the dication by the electron beam upon the XPS experiment.[7] The XPS of the powder exhibits similar signals although longer irradiation times are needed to clearly visualized the peaks corresponding to the reduced species.
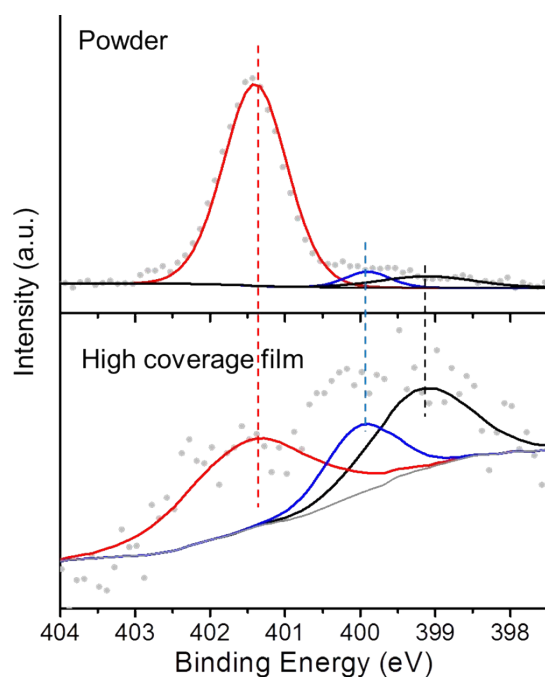
Figure S6. N1s photoemission spectrum of [**1**](BF$_4$) in powder and incorporated in an LB film.

Equipment used to characterize the Langmuir and LB films

Surface potential measurements were carried out using a Kelvin Probe provided by Nanofilm Technologie GmbH, Göttingen, Germany. During monolayer compression, π-A and ΔV-A isotherms were recorded simultaneously.

A commercial mini-Brewster angle microscope (mini-BAM) from Nanofilm Technologie GmbH, Göttingen, Germany, was employed for the direct visualization of the monolayers at the air-water interface and a commercial UV-vis reflection spectrophotometer, details described elsewhere,[2] was used to obtain the reflection spectra of the Langmuir films during the compression process.

Atomic force microscopy (AFM) experiments were performed using a Multimode 8 microscope equipped with a Nanoscope V control unit from Bruker. Tapping mode was used in ambient air conditions with a scan rate of 1 Hz with a silicon cantilever supplied by Bruker, RTESPA-150 (90-210 kHz, and 5 N·m^{-1},and nominal tip radius of 8 nm).

Quartz crystal microbalance (QCM) measurements were carried out using a Stanford Research System instrument and employing AT-cut, α-quartz crystals with a resonant frequency of 5 MHz having circular gold electrodes patterned on both sides.

UV-vis spectra of the solutions and LB monolayers were acquired on a Varian Cary 50 spectrophotometer and recorded using a normal incident angle with respect to the film plane.

Cyclic voltammetry (CV) experiments were carried out using an Autolab potentiostat from Eco Chemie and a standard three electrode cell, where the working electrode was a gold electrode purchased from Arrandee® (bare gold or covered by a SAM of **1**) connected to the potentiostat by means of a cable terminated in a metallic crocodile clip that held the electrode.[8] The reference electrode was Ag/AgCl, KCl (3M), and the counter electrode was a Pt sheet.

X-ray photoelectron spectroscopy (XPS) spectra were acquired on a Kratos AXIS ultra DLD spectrometer with a monochromatic Al Kα X-ray source (1486.6 eV) using a pass energy of 20 eV. To provide a precise energy calibration, the XPS binding energies were referenced to the C1s peak at 284.6 eV.

Single molecule and LB films conductance measurements

Agilent STM running Picoscan 5.3.3 software was used for all single molecule and LB films electrical conductance measurements, which were performed at room temperature in air. Molecular ad-layers were formed on Au(111) textured substrates. These commercially available (Arrandee) substrates were produced from gold on glass samples with a chromium adhesive layer and were flame annealed immediately prior to use. Flame annealing involved gently heating the gold slide until it developed a slight orange glow. It was then retained in this state for about 30 s, with care being taken to ensure that the gold film sample did not overheat. Molecular adsorption for single molecule conductance measurements was achieved by placing the gold electrode in a $5 \cdot 10^{-4}$ M solution of $[\mathbf{1}](BF_4)_2$ in ethanol for 60 s. Gold STM tips were freshly prepared for each experiment by etching of a 0.25 mm Au wire (99.99%) in a mixture of HCl (50%) and ethanol (50%) at +2.4 V.

In the *I*(*s*) technique, the STM tip is moved toward the surface to a close distance determined by the STM set point conditions. Metallic contact between tip and surface, is avoided and from the step-point conditions the STM tip is rapidly retracted.[9-11] In these measurements, the *I*(*s*) process involves repeating this cycle many times for the statistical analysis of conductance data. A fraction of the approach/retraction cycles lead to the formation of molecular bridges and such junction formation events are recognized during the retraction process as current steps. These steps, where the current rapidly decays to the noise platform, are characteristic of the cleavage of Au-molecule(s)-Au electrical junctions. At least 500 such junction forming scans, with plateaus longer than 0.1 nm, were recorded and used in the statistical (histogram) analysis. *I*(*s*) traces are not included for scans where there are no characteristic junction cleavage steps to avoid the ambiguity of inclusion of traces where no molecular junction is formed. In these measurements the tip potential is referred to as U_t.

Details of the tip to substrate calibration in the *I*(*s*) technique

In order to construct 2D histograms the distance on the x-axis was adjusted for the initial tip-substrate distance (s_0) at the start of the *I*(*s*) retraction. This follows the method reported previously[11-15], where it is necessary to obtain a quantification of the current decay as expressed by (d ln*I*/d*s*). To achieve this only *I*(*s*) traces were selected which featured a monotonic exponential decay of the tunneling current (Figure S5a). The collected data were plotted as ln*I* vs. *s* (Figure S5b). After averaging the slope of this plot d ln*I*/d*s* values typically in the range of (7.56±0.33) and (6.74±0.51) nm^{-1} were obtained for low coverage and LB films, respectively. These values agree well with those reported for similar molecular films of highly conjugated compounds[16, 17] and for single molecules.[12, 13] The resulting d ln*I*/d*s* value is then used in Equation (4) to obtain the distance at the start of the *I*(*s*) trace. This procedure can be viewed as an extrapolation of the conductance to the value when the gold STM tip contacts the gold substrate at a atom single point. It is assumed that this metal-to-metal point contact results in gold atom point contact conductance, $G_0 = 2e^2/h \approx 77.4$ μS, sometimes referred to as the "quantum conductance" in molecular electronics. Using I_0=30 nA and U_t=0.6 V as set point parameters, the estimated s_0 values were 1.09 and 1.03 nm for low coverage and LB films, respectively. For the LB film, comparing this experimentally estimated s_0 value with the monolayer thickness, which is obtained by considering the

molecular inclination in the film (1.50 nm, Figure 4), the tip is determined to be embedded in the monolayer at the beginning of each scan.

$$s_0 = \frac{ln\left(G_0 U_t/I_0\right)}{dln(I)/ds}$$

(4)
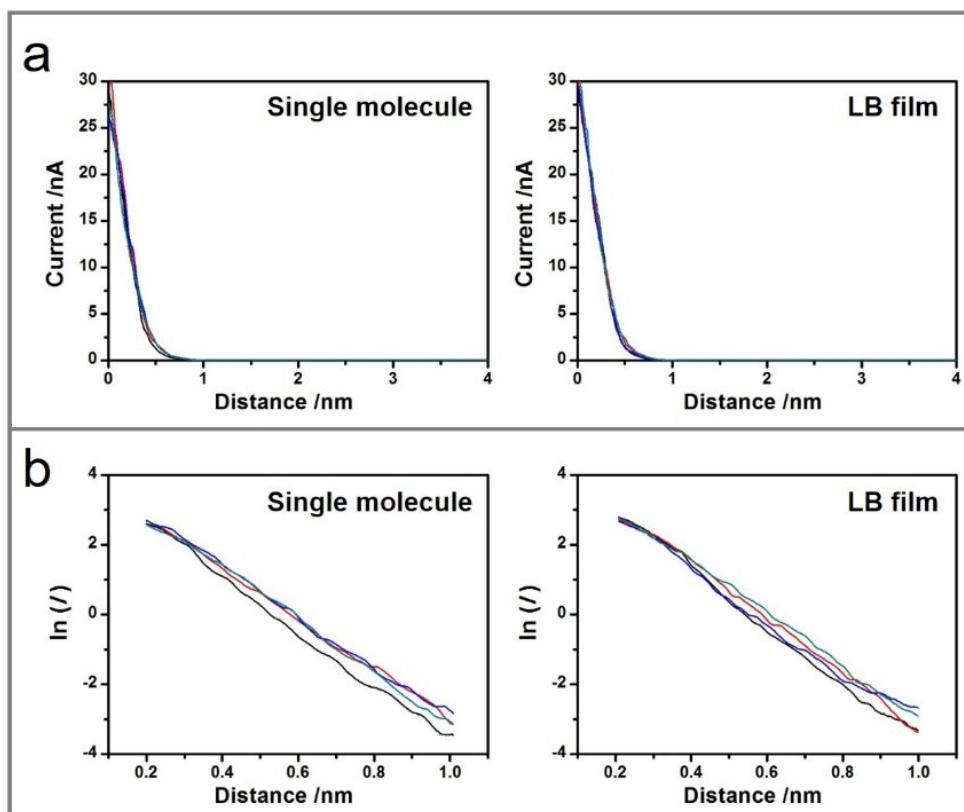
Figure S5. a) Representative $I(s)$ traces, in which the tunneling current shows a monotonic exponential decay, used for the calibration of tip-substrate distance. b) ln$I$ vs. s plots used to evaluate the dln$I$/ds values.

Single molecule measurements of 2^{2+} and 3

Conductance measurements of molecular junctions formed from either 2^{2+} or **3** were carried out also using a scanning tunneling microscopy (STM) by means of the $I(s)$ method. Figure S6 shows typical conductance-distance, $I(s)$, curves for junctions formed by a single molecule of 2^{2+} (a) or **3** (b) as well as the conductance histogram constructed from 500 experimental $I(s)$ curves. $I(s)$ curves of a single molecule of 2^{2+} feature a set of plateaus with a conductance value at $(5.3 \pm 0.70) \times 10^{-5}\ G_0$, meanwhile for **3** a set of plateaus with a conductance value at $(1.25 \pm 0.50) \times 10^{-5}\ G_0$ is observed.
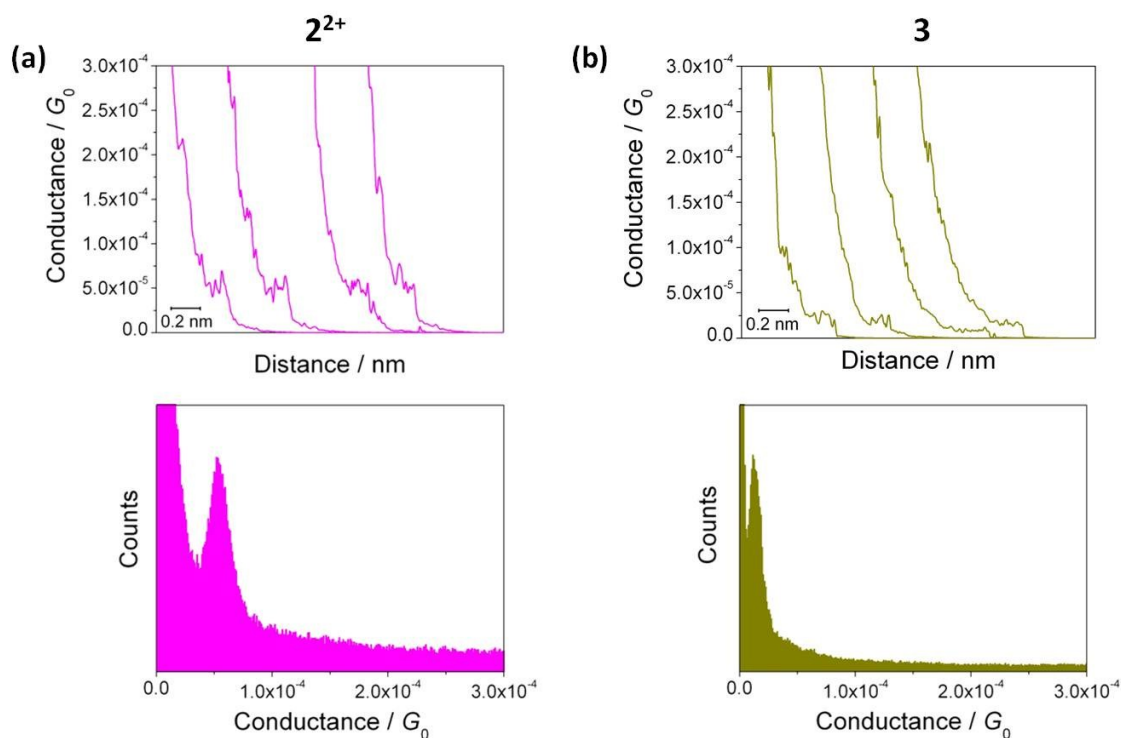
Figure S6. (a) Representative *I*(*s*) traces for single molecule junctions of **2²⁺** and conductance histogram built from summation of conductance traces (ca. 500) that show discernible plateaus. (b) Representative *I*(*s*) traces for single molecule junctions of **3** and a conductance histogram built from summation of conductance traces (ca. 500) that shows discernible plateaus. U_t = 0.6 V where U_t is the "*tip bias*".

Determination of the thickness of the LB film of [1](BF4)2 by AFM measurements

The average thickness of the LB film of $[1](BF_4)_2$ was obtained by scratching the organic layer with the AFM tip in a (500 x 125) nm² area. Then, by subtracting the height of the bare substrate (unveiled after removing the organic film) from that of the surrounding molecule layer, the thickness of the film was obtained.[18] Accordingly, a representative cross section together with a detailed statistical analysis of the height distributions corresponding to the organic layer and the bare Au(111) surfaces are depicted in Figure S6(c) and (d), respectively. Both contributions are fitted separately to Gaussian functions whose maximum difference allows an accurate estimation of the layer thickness, i.e. 1.4 ± 0.2 nm.
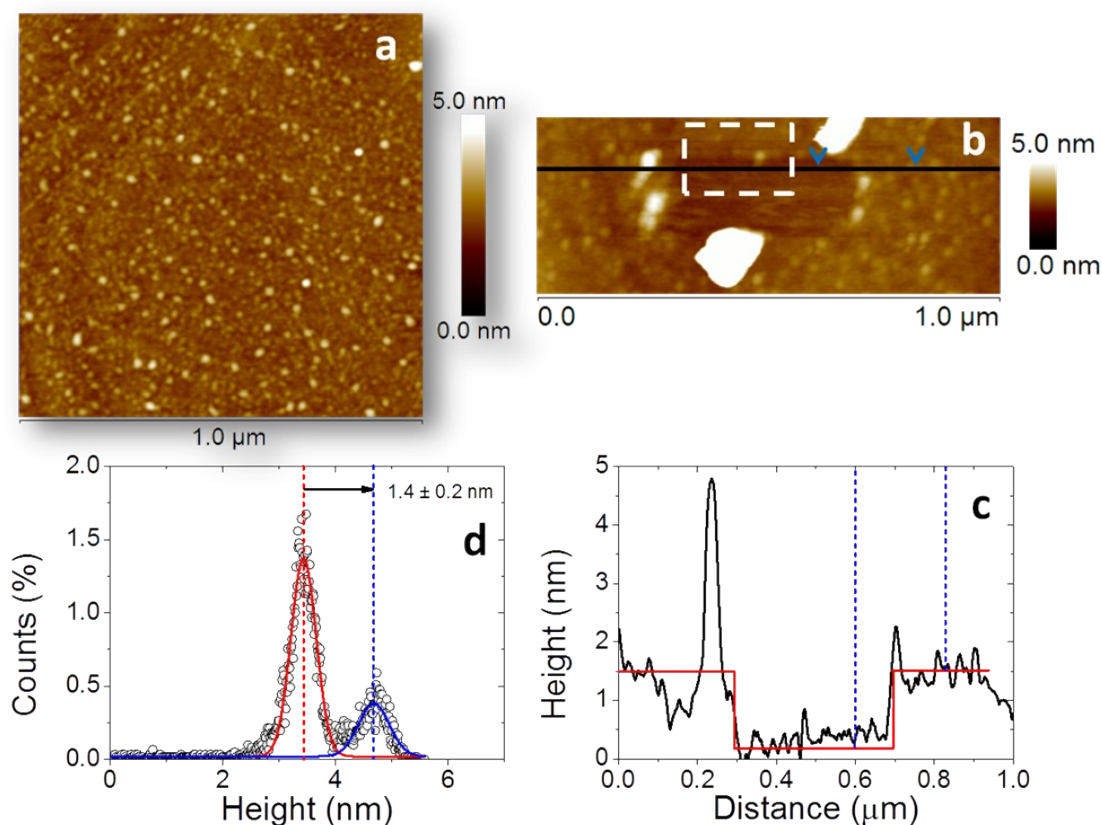
Figure S7. (1.0 x 1.0) μm² AFM image showing the topography of an monomolecular film of $\mathbf{1^{2+}}$ formed on a Au(111) surface (a). (1.0 x 1.0) μm² AFM image of a (500 x 125) nm² rectangular scratch made in a smooth Au(111) terrace covered by the organic layer (b), and a representative cross-section profile across the scratch (c). Depth profile histogram corresponding to the dashed white-boxed (300 x 50) nm² area, exhibiting the height value distributions related to bare Au(111) and a monomolecular LB film of $\mathbf{1^{2+}}$ (d). From the height difference between the two maximums of the Gaussian fits, the thickness of the film, i.e. 1.4 ± 0.2 nm, can be estimated.

References

1. S. Martin, P. Cea, C. Lafuente, H. M. Royo, M. C. Lopez, Surface Science, 2004, **563**, 27.
2. S. Martin, A. Villares, M. Haro, M. C. Lopez, P. Cea, J Electroanal Chem, 2005, **578**, 203.
3. P. Cea, C. Lafuente, J. S. Urieta, M. C. Lopez, F. M. Royo, Langmuir, 1998, **14**, 7306.
4. G. Sauerbrey, Z Phys, 1959, **155**, 206.
5. H. Gruniger, D. Mobius, H. Meyer, J Chem Phys, 1983, **79**, 3701.
6. W. H. Yu, Y. Xhang, E. T. Kang, K. G. Neoh, S. Y. Wu, Y. F. Chow, J. Electrochem. Soc., 2003, **8**, F156.
7. S. Breuer, D. T. Pham, S. Huemann, K. Gentz, C. Zoerlein, R. Hunger, K. Wandelt, P. Broekmann, New J. Phys., 2008, **10**, 125033 (24pp).

8.   P. Cea, S. Martín, A. González-Orive, H. M. Osorio, P. Quintín, L. Herrer, J. Chem. Ed., 2016, **93**, 1441.
9.   W. Haiss, R. J. Nichols, H. van Zalinge, S. J. Higgins, D. Bethell, D. J. Schiffrin, Phys Chem Chem Phys, 2004, **6**, 4330.
10. W. Haiss, H. van Zalinge, S. J. Higgins, D. Bethell, H. Hobenreich, D. J. Schiffrin, R. J. Nichols, J Am Chem Soc, 2003, **125**, 15294.
11. R. J. Nichols, W. Haiss, S. J. Higgins, E. Leary, S. Martin, D. Bethell, Phys Chem Chem Phys, 2010, **12**, 2801.
12. S. Martin, I. Grace, M. R. Bryce, C. S. Wang, R. Jitchati, A. S. Batsanov, S. J. Higgins, C. J. Lambert, R. J. Nichols, J Am Chem Soc, 2010, **132**, 9157.
13. W. Haiss, C. S. Wang, I. Grace, A. S. Batsanov, D. J. Schiffrin, S. J. Higgins, M. R. Bryce, C. J. Lambert, R. J. Nichols, Nat Mater, 2006, **5**, 995.
14. W. Haiss, S. Martin, E. Leary, H. van Zalinge, S. J. Higgins, L. Bouffier, R. J. Nichols, J Phys Chem C, 2009, **113**, 5823.
15. G. Sedghi, K. Sawada, L. J. Esdaile, M. Hoffmann, H. L. Anderson, D. Bethell, W. Haiss, S. J. Higgins, R. J. Nichols, J Am Chem Soc, 2008, **130**, 8582.
16. L. M. Ballesteros, S. Martin, J. Cortes, S. Marques-Gonzalez, S. J. Higgins, R. J. Nichols, P. J. Low, P. Cea, Chem-Eur J, 2013, **19**, 5352.
17. G. Pera, S. Martin, L. M. Ballesteros, A. J. Hope, P. J. Low, R. J. Nichols, P. Cea, Chem-Eur J, 2010, **16**, 13398.
18. F. Anariba, S. H. DuVall, R. L. McCreery, Anal Chem, 2003, **75**, 3837.